Journal of Colloid and Interface Science 381 (2012) 89–99

Contents lists available at SciVerse ScienceDirect

Journal of Colloid and Interface Science

www.elsevier.com/locate/jcis

Structural behaviour of mixed cationic surfactant micelles: A small-angle neutron scattering study

L. Magnus Bergström [a,*], Vasil M. Garamus [b]

[a] KTH Royal Institute of Technology, School of Chemical Science and Engineering, Department of Chemistry, Surface and Corrosion Science, SE-100 44 Stockholm, Sweden
[b] Helmholtz-Zentrum Geesthacht, Centre for Materials and Coastal Research, D-215 02 Geesthacht, Germany

ARTICLE INFO

Article history:
Received 6 March 2012
Accepted 10 May 2012
Available online 18 May 2012

Keywords:
Surfactants
Mixed micelles
Small-angle neutron scattering
Bending elasticity

ABSTRACT

Self-assembly in mixtures of two single-chain cationic surfactants, with different tail lengths (CTAB and DTAB) as well as of a single-chain (DTAB) and a double-chain (DDAB) cationic surfactant, with identical tail lengths, have been investigated with small-angle neutron scattering (SANS) and rationalised in terms of bending elasticity properties. The growth behaviour of micelles with respect to surfactant composition appears completely different in the two surfactant mixtures. DTAB form small oblate spheroidal micelles in presence of [NaBr] = 0.1 M that transform into prolate spheroidal mixed CTAB/DTAB micelles upon adding moderate amounts of CTAB, so as to give a mole fraction $y = 0.20$ in solution. Most unexpectedly, upon further addition of CTAB the mixed CTAB/DTAB micelles grow with an almost equal rate in both length and width directions to form tablets. In contrast to this behaviour, mixed DDAB/DTAB micelles grow virtually exclusively in the length direction, in presence of [NaBr] = 0.1 M, to form elongated ellipsoidal (tablet-shaped) and subsequently long wormlike micelles as the fraction of DDAB in the micelles increases. Mixed DDAB/DTAB micelles grow to become as long as 2000 Å before an abrupt transition to large bilayer structures occurs. This means that the micelles are much longer at the micelle-to-bilayer transition as compared to the same mixture in absence of added salt. It is found that the point of transition from micelles to bilayers is significantly shifted towards higher fractions of aggregated DTAB as an appreciable amount of salt is added to DDAB/DTAB mixtures, indicating a considerable reduction of the spontaneous curvature with an increasing [NaBr]. By means of deducing the various bending elasticity constants from our experimental results, according to a novel approach by ours, we are able to conclude that the different growth behaviours appear as a consequence of a considerably lower bending rigidity, as well as higher saddle-splay constant, for DDAB/DTAB surfactant mixtures in presence of [NaBr] = 0.1 M, as compared to mixtures of CTAB/DTAB in [NaBr] = 0.1 M and DDAB/DTAB in absence of added salt.

1. Introduction

The hydrophobic effect, i.e. the principle that hydrophobic substances are readily soluble in most nonpolar solvents, but only sparingly soluble in water, is the single most important factor that causes surfactant molecules to self-assemble to micelles and bilayers in an aqueous solvent [1]. As a result of the high free energy penalty associated with the formation of the unfavourable hydrocarbon–water contact area, the hydrocarbon tails of the surfactant molecules self-associate to form a geometrically well-defined hydrophobic interior core of micelles and bilayers with virtually no water penetration. For the case of ionic surfactants Gruen summarised this so called standard picture of micelles in three points: (i) each aggregated surfactant has almost all of its tail in the micelle core, (ii) head groups and solvent are almost totally excluded from the micelle core, and (iii) the surfactant tails are conformationally disordered (liquid-like) and fill the core at approximately liquid density throughout [2]. It is well-known that simple geometrical considerations imply that most common small compact micelles cannot be spherically shaped but must assume some kind of biaxial (prolate or oblate) spheroidal or triaxial ellipsoidal shape [3,4].

Pure micelles formed from three different cationic surfactants dodecyltrimethylammonium bromide (DTAB), tetradecyltrimethylammonium bromide (TTAB) and hexadecyltrimethylammonium bromide (CTAB) were originally investigated by Berr using small-angle neutron scattering (SANS) in the range of scattering vectors $0.025\ Å^{-1} < q < 0.25\ Å^{-1}$ [5]. The data were analysed with a core–shell model for prolate spheroidal micelles and it was concluded that a substantial amount of water penetrates into the micelle hydrocarbon core, i.e. 4.3, 2.3 and 2.6 methylene groups mix with water in a Stern layer for DTAB, TTAB and CTAB, respectively. Later on, SANS data for sodium dodecylsulphate (SDS) and lithium dodecylsulphate (LDS) in different electrolyte concentrations were fitted using a (core–shell) model for oblate spheroidal micelles [6].

* Corresponding author. Fax: +46 8 20 82 84.
E-mail address: magnusbe@kth.se (L. Magnus Bergström).

0021-9797/$ - see front matter © 2012 Elsevier Inc. All rights reserved.
http://dx.doi.org/10.1016/j.jcis.2012.05.015

The growth behaviour of pure SDS and DTAB micelles as a function of concentration of added NaBr were investigated with SANS in the range 0.004 $Å^{-1} < q < 0.5$ $Å^{-1}$ [7]. Several models were considered and the agreement between each model and data were compared. In accordance, it was concluded that both SDS and DTAB micelles were shaped as oblate spheroids that may grow into triaxial general ellipsoids upon increasing the electrolyte concentration. The scattering data were fitted with models assuming the aggregates to have a homogenous and uniform scattering length density and the model fits could not be further improved by means of employing a core–shell model. This is consistent with the fact that the sulphate head group of SDS has a considerably lower contrast to the solvent (D_2O) than the hydrophobic tail and, as a consequence, it is not visible with the SANS technique. This is confirmed by the fact that deuterated SDS dissolved in deuterium oxide is completely invisible in SANS data spectra [8]. The trimethylammonium head group of DTAB, on the other hand, has a very similar scattering length density as the alkyl tails and is small in size. This means that, from a neutron scattering perspective, DTAB micelles are shaped as compact oblates with small head groups protruding from the micelle interface. A homogeneous micelle core consisting of pure hydrocarbon, having a strong contrast with the solvent (D_2O), is consistent with the standard picture of surfactant micelles. An oblate rather than prolate spheroidal shape is supported by the very small growth rates with respect to surfactant concentration observed for SDS and DTAB micelles, respectively, using time-resolved fluorescence quenching (TRFQ) [9,10]. Moreover, the diffusion behaviour of SDS micelles in [NaCl] = 0.1 M have been demonstrated to be consistent with oblate spheroidal shape [11].

General ellipsoidal micelles have been observed with SANS in mixtures of SDS and the zwitterionic surfactant tetradecyltrimethylamine oxide (TDMAO) [12], SDS/DTAB mixtures [13,14] as well as in mixtures of SDS and the double-chain cationic surfactant didodecyl dimethylammonium bromide (DDAB) [15]. More recently, pure micelles formed by the cationic surfactant hexadecyltrimtehylammonium chloride (CTAC) were found to form oblate spheroidal micelles using SANS [16].

Micelles formed in mixtures of the single-chain cationic surfactant DTAB and the double-chain cationic surfactant DDAB was first investigated with SANS by Lusvardi et al. [17] at scattering vectors ranging up to $q = 0.22$ $Å^{-1}$. However, only prolate spheroidal shape was considered in the data analysis. More recently, the growth behaviour with respect to surfactant composition of mixed DTAB/DDAB micelles in absence of added salt was investigated with SANS by the present authors [18]. It was found that the quality of the model fits could be significantly improved using a model for general ellipsoids. In accordance, it was concluded that rather small oblate spheroidal DTAB micelles grow slightly in width, and more pronouncedly in the length direction, to form general ellipsoidal micelles as an increasing amount of DDAB was incorporated in the surfactant aggregates. When the ellipsoidal micelles have a half axis related to length equal to $c = 70$ Å, bilayer discs and vesicles abruptly begin to form and are observed to coexist with the micelles in a narrow regime. From model calculations based on the Poisson–Boltzmann mean field theory, we were able to determine the mole fraction of DDAB in the self-assembled interfacial aggregates (i.e., micelles and bilayers) at the micelle-to-bilayer transition equal to $x = 0.41$ in H_2O (with static light scattering) [19] and $x = 0.48$ in D_2O (with SANS) [18].

The growth of micelles and the transition from micelles to bilayers or bilayer vesicles in two different surfactant mixtures have recently been investigated with SANS by Grillo et al. [20,21]. Micelles formed in mixtures of the nonionic surfactant monododecyl ether ($C_{12}E_4$) and DDAB were analysed with a core–shell model for spheroidal micelles, whereas micelles formed in mixtures of $C_{12}E_4$ and the double chain anionic surfactant AOT were analysed with models for either spheres or cylinders.

The structural behaviour in surfactant systems has previously been most commonly rationalised with arguments based on rather simple geometrical packing constraints of the aggregated surfactant molecules, in terms of the so called critical packing parameter $cpp = va/l_c$ [22]. v is the volume and l_c is the length, respectively, of the hydrocarbon part of the surfactant, whereas a is the area per molecule at the hydrocarbon/solvent interface including head groups as well as solvent molecules mixed with one another just outside the hydrophobic core. The purpose of the *cpp* parameter is to deduce geometrical size and shape of the aggregate from properties of the single surfactant molecules and, in order to do so, it is of crucial importance that a is a property of the single molecules. However, a depends on the mean and Gaussian curvatures, H an K, respectively, of the self-assembled interfacial aggregate according to the following relation [22,23]

$$\frac{1}{a(H,K)} = \frac{\xi}{v}\left(1 - \xi H + \frac{\xi^2}{3}K\right) \tag{1}$$

where ξ is the thickness of the self-assembled monolayer interface. This means that a must be a property of the self-assembled interfacial aggregate with curvature [H, K] rather than of the bare surfactant molecule. As a consequence, any attempt to predict aggregate geometrical size and shape (which is equivalent to curvature) from molecular surfactant properties must fail and usually ends up in a circular argumentation where a value of a, based on aggregate properties, is chosen to calculate *cpp* from which the very same aggregate properties is supposed to be deduced.

Moreover, several aspects of the structural behaviour of self-assembled interfacial aggregates can neither be explained nor rationalised using the *cpp* parameter. For instance, the growth rate of pure surfactant micelles with respect to surfactant concentration may differ considerably depending on the chemical structure of the surfactant [24–26]. Likewise, micelles formed by either SDS [7] or CTAB [27] grow rapidly in length with an increasing electrolyte concentration to form long wormlike micelles whereas the influence of added salt on, for instance, DTAB [7,10] or sodium octylsulphate (SOS) [28] micelles is considerably less pronounced. Micelles tend to more or less abruptly transform into bilayers at some certain surfactant composition [18,20,21,29–31], and the size of the micelles at the point of transition may differ considerably for different surfactant mixtures. For instance, rather small globular SOS-rich micelles have been observed to abruptly transform into vesicles whereas long threadlike CTAB-rich micelles transform into vesicles in mixtures of the anionic surfactant SOS and the cationic surfactant CTAB [28].

In order to account for the different behaviours of various surfactant mixtures, we have recently set up a theory for general triaxial micelles by means of combining thermodynamics of self-assembly with bending elasticity theory [18,32]. The theoretical approach introduces the three bending elasticity constants spontaneous curvature (H_0), bending rigidity (k_c) and saddle-splay constant ($\bar{k}_c$).

In the present paper we investigate two surfactant mixtures that display completely different micelle growth behaviours with respect to width and length as function of surfactant composition. We have chosen to study mixtures of a single-chain and a double-chain cationic surfactant (DTAB and DDAB), as well as mixtures of two single-chain surfactants with different tail lengths (CTAB and DTAB), in presence of [NaBr] = 0.1 M. In particular, we want to correlate the different growth behaviours, and the fact that in certain systems micelles may grow into very long wormlike micelles whereas in other cases they remain rather small and compact, with the detailed geometrical shape of the micelles. For the first time we

compare and rationalise the structural behaviours of some different surfactant mixtures by means of employing our recently developed approach to deduce the three bending elasticity constants H_0, k_c and $\bar{k}_c$ from experimental results. Although CTAB and DTAB are two very common cationic surfactants, mixed micelles formed by these surfactants have, to our knowledge, never been investigated before. Likewise, mixed DDAB/DTAB micelles in presence of large amounts of electrolyte have never been investigated before with SANS.

2. Materials and methods

2.1. Materials

Dodecyltrimethylammonium bromide (>99%, GC) was obtained from Sigma, didodecyldimethylammounium bromide (>98%, GC) from Fluka, hexadecyltrimethylammonium bromide (>98%, GC) from Sigma and sodium bromide (>99.5%, GC) from Fluka. All surfactants were used without further purification. Deuterium oxide (D_2O) with 99.9 atom% D was purchased from Aldrich Chemical Company.

2.2. Sample preparation

Stock solutions containing dodecyltrimethylammonium bromide (DTAB) and didodecyldimethylammounium bromide (DDAB) in [NaBr] = 0.1 M, with different surfactant compositions ranging from $y \equiv [\text{DDAB}]/([\text{DDAB}] + [\text{DTAB}]) = 0$ to $y = 0.25$, were prepared by simply mixing the surfactants with deuterium oxide to yield an overall surfactant concentration $c_t = [\text{DDAB}] + [\text{DTAB}] = 30$ mM. Stock solutions containing DTAB and hexadecyltrimethylammonium bromide (CTAB), with [CTAB] + [DTAB] = 30 mM, were prepared in an identical way. The final samples were obtained by means of diluting the stock solutions with deuterium oxide to obtain a total surfactant concentration $c_t = 15$ and 7.5 mM, respectively. To avoid formation of precipitate we have carried out all our measurements at 30 °C (the Krafft point of CTAB in [NaBr] = 0.1 M in D_2O is 29 °C). All samples were equilibrated at 30 °C at least 7 days before measured. Deuterium oxide (D_2O) was chosen as solvent in order to minimise the incoherent background from hydrogen and obtain a high scattering contrast.

2.3. Methods

Small-angle neutron scattering (SANS) experiments were carried out at the SANS-1 instrument at the Geesthach Neutron Facility GeNF, Geesthacht, Germany. A range of magnitudes of the scattering vector q from 0.005 to 0.25 Å^{-1} was covered by three or four combinations of sample-to-detector distances (0.7–9.7 m) at a neutron wavelength of 8.5 Å. The wavelength resolution was $\Delta\lambda/\lambda = 10\%$ (full-width-at-half-maximum value).

The samples were kept in quartz cells (Hellma) with a path length of 2 mm. The raw spectra were corrected for background from the solvent, sample cell and other sources by conventional procedures [33]. The SANS data were set to absolute scale units according to procedures described in the Supporting information. The scattering intensity was normalised by means of dividing with the concentrations in g/mL of solute (DTAB, DDAB and CTAB), giving the unit [mL g^{-1} cm^{-1}] for the normalised scattering intensity $(d\sigma/d\Omega)/c_t$.

Throughout the data analyses corrections were made for instrumental smearing. For each instrumental setting the ideal model scattering curves were smeared by the appropriate Gaussian resolution function when the model scattering intensity was compared with the measured absolute scale intensity in least-square model fitting data analysis. Details for the smearing procedure may be found elsewhere [34,35]. The parameters in the model were optimised by means of conventional least-squares analysis and the quality of the fits was measured in terms of the reduced chi-squared parameter (χ^2) [36,37]. The errors of the parameters were calculated by conventional methods [36,37]. More details are given in the Supporting information.

The average excess scattering length density per unit mass of solute for DTAB in D_2O, $\Delta\rho_m = -6.37 \times 10^{10}$ cm/g, was calculated using the appropriate molecular volume $\hat{v} = 491$ Å^3 and molecular weight $M_w = 308.35$ g/mol of the surfactant monomer [38,39]. The corresponding quantities for DDAB are $\Delta\rho_m = -7.01 \times 10^{10}$ cm/g, $\hat{v} = 810$ Å^3 and $M_w = 462.65$ g/mol and for CTAB $\Delta\rho_m = -6.66 \times 10^{10}$ cm/g, $\hat{v} = 607$ Å^3 and $M_w = 364.45$ g/mol [38,39]. The scattering length density of mixed micelles has been set to $\Delta\rho_{mix} = x\Delta\rho_1 + (1-x)\Delta\rho_2$, where x is the mole fraction of surfactant in the aggregates. x is calculated according to a procedure introduced in a recent paper by ours [19] and briefly discussed in Supporting information.

For one transparent sample, containing large wormlike micelles, we have carried out static light scattering (SLS) measurements with a BI-200SM goniometer from Brookhaven Instruments attached to a water-cooled Lexel 95-2 laser with maximum power of 2 W and wavelength 514.5 nm. Experiments were carried out at 29 different angles in the range of $15^\circ \leqslant \theta \leqslant 155^\circ$, corresponding to q values in the range of 4.26×10^{-4} Å^{-1} $\leqslant q \leqslant 31.8 \times 10^{-4}$ Å^{-1}. For each angle the sample was measured a maximum of fifteen individual times out of which the five with the lowest intensities were picked out and subsequently averaged. The SLS data were then converted to absolute neutron units using toluene as a reference standard, with the appropriate refractive index increments, before combined and analysed together with SANS data. The refractive index increment $dn/dc = 0.153$ mL/g for both DTAB and DDAB at the appropriate laser light wavelength [19].

3. Data analyses

The different models used in the least-square model fitting data analysis are given in Supporting information. Rather small and compact micelles are formed in DDAB/DTAB mixtures with high fractions of DTAB, as well as in all CTAB/DTAB mixtures, and the corresponding SANS data were best fitted using a model for triaxial general ellipsoids with half axis a, b and c, where $a < b < c$. This model consistently gives a significantly better agreement with data than a biaxial spheroidal model, except for a few samples in which the micelles turn into (oblate or prolate) biaxial spheroids as special cases. One typical example of SANS data, and a least-square fit with a model for general ellipsoids, is shown in Fig. 1. For the sake of comparison, we have also included a model for monodisperse spheres in Fig. 1. It is clearly seen that the model for monodisperse spheres deviates considerably from the scattering data in the high-q regime. However, the quality of the model fit for spherical micelles may be considerably improved by means of allowing for a substantial polydispersity of the spherical micelles [7,40]. Nevertheless, the quality of the polydisperse sphere model fit, as measured by χ^2, is slightly but consistently worse for all samples as compared with the ellipsoidal model. Moreover, a comparatively large polydispersity, i.e. a relative standard deviation $\sigma/\langle R\rangle = 0.24$ and an average radius $\langle R\rangle = 23.6$ Å for the example in Fig. 1 ($y = [\text{CTAB}]/([\text{CTAB}] + [\text{DTAB}]) = 0.80$ and [CTAB] + [DTAB] = 30 mM), is required to generate an acceptable quality of the model fit. This model fitting result corresponds to a distribution of spherical micelles where more than 5% have a radius larger than $R = 33$ Å and more than 1% of the micelles have $R > 37$ Å. These values should be compared with the length $l_{max} = 21.7$ Å of a fully stretched out ali-

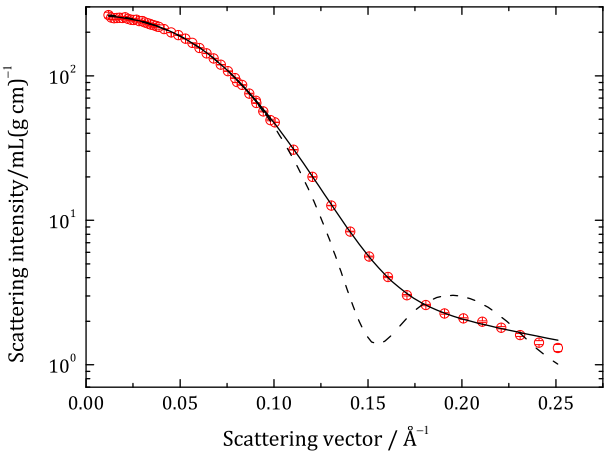

Fig. 1. Normalised scattering cross section $(d\sigma/d\Omega)/c_t$ as a function of the scattering vector q for mixtures of DTAB and CTAB in [NaBr] = 0.1 M in D_2O for a given total surfactant concentration c_t = [CTAB] + [DTAB] = 30 mM and composition y = [CTAB]/([CTAB] + [DTAB]) = 0.80. Individual symbols represent SANS data obtained for different sample-detector distances. The lines represent the best available fit with a model for general ellipsoids (solid line) and monodisperse spheres (dashed line). The quality of the fits as measured by χ^2 are 4.4 (solid line) and 1074 (dashed line). The spatial dimensions of the ellipsoids, as obtained from the model fitting analysis, are a = 19.9 ± 0.2 Å, b = 29.4 ± 0.3 Å and c = 40.3 ± 0.4 Å. A model for polydisperse spheres with an average radius $\langle R\rangle$ = 23.6 Å and relative standard deviation $\sigma/\langle R\rangle$ = 0.24 gives an agreement between model and data equal to χ^2 = 5.0.

phatic C_{16} chain (which is the tail of the longest surfactant CTAB in the mixture) [1]. The contribution from the head groups is not expected to be larger than about 3–4 Å. Hence, we may conclude that the polydisperse sphere model is inconsistent with simple geometrical considerations since the spherical micelles must have a radius considerably larger than the length of a fully stretched CTAB molecule. Moreover, fluctuations in size of spherical micelles are expected to be disfavoured by an energetic penalty to change the local curvature of a micelle and, as a result, the polydipsersity of spherical micelles is expected to be very low. Theoretically estimated values of $\sigma R/\langle R\rangle$ for spherical micelles have been found to be less than about 0.05 [41].

The quality of the model fits in the low-q range were significantly improved by means of using a structure factor $S(q)$ as derived by Hayter and Penfold [42] from the Ornstein–Zernike equation in the rescaled mean spherical approximation [43], together with a so-called decoupling approximation [44,45] valid for particles with small anisotropy. However, it was found that the double layer interaction part has a negligible contribution to this structure factor in the high electrolyte concentrations we have investigated, i.e. [NaBr] = 0.1 M and, as a result, the charge of the micelles could not be reliably determined from our model fitting analysis. Hence, in the fitting procedure the model fit was optimised with respect to volume fraction of micelles in addition to the three half axes a, b and c. The obtained volume fraction of micelles ($0.01 \lesssim \phi_{mic} \lesssim 0.02$) correspond to surfactant concentrations in the range 30–60 mM, i.e. somewhat larger than the actual surfactant concentrations. This indicates that repulsive electrostatic double layer interactions, or the fact that the micelles do not strictly behave as hard spheres, may have a non-negligible impact on the structure factor. By means of introducing an additional fitting parameter related to inter-micellar interactions, we are able to improve the quality of our model fits, thus making our obtained spatial dimensions more reliable.

Substantially elongated and polydisperse micelles are formed in mixtures with y = [DDAB]/([DDAB + [DTAB]) = 0.15 as well as by pure CTAB in [NaBr] = 0.1 M, and the corresponding SANS data were best fitted with a model for polydisperse rigid rods [7,14,46]. As the micelles grow further in length they become slightly flexible. In accordance, the model fits could be significantly improved using a form factor for polydisperse self-avoiding wormlike micelles with a contour length L and persistence length l_p [47]. The polydisperse rodlike and wormlike micelles were found to have values of $\sigma_L/\langle L\rangle$ close to or slightly below unity, but it is difficult to determine its exact value from the model fitting procedure. For this reason, $\sigma_L/\langle L\rangle$ was consistently fixed to equal 0.95. Inter-micellar excluded volume interactions are difficult to take into account for considerably elongated rods and worms and was neglected in our model fitting data analyses. Because of the comparatively large amounts of electrolyte present in our samples ([NaBr] = 0.1 M), effects due to electrostatic double layer interactions between micelles are expected to be negligible. However, significant excluded volume interactions may still contribute non-negligibly to micellar interference effects and, as a consequence, the average micelle length $\langle L\rangle$ as obtained from our data analysis is expected to be somewhat smaller than the real length of the micelles.

It is not possible to distinguish an elliptical cross-section from polydispersity of a strictly circular cross-section for rodlike or wormlike micelles from the quality of our model fits. However, micelles tend to fluctuate significantly only in so far as the local curvature is not influenced. For instance, fluctuations in the length direction of rodlike or wormlike micelles do not influence the local curvature and have been observed to be substantial in magnitude [22,48,49]. On the other hand, fluctuations in radius of a strictly circular cross-section are expected to be small as a result of the energetic penalty of changing the local curvature of strictly cylindrical micelles. The energetic penalty has been found to be enhanced by effects due to chain conformation entropy [49,50]. As a result, we have interpreted our results in terms of an elliptical cross-section of the rodlike micelles. This interpretation is consistent with our observation that more compact and less elongated micelles were best fitted with a model for triaxial ellipsoids.

Similar to our earlier studies where alkyltrimethylammonium bromide micelles were analysed with an ellipsoidal or spheroidal model [7,14,15,18], the quality of the model fits could not be improved by means of employing a core–shell model.

4. Results and discussion

4.1. Mixtures of DDAB and DTAB in [NaBr] = 0.1 M

Examples of SANS data together with model fits for micelles formed by DDAB and DTAB in [NaBr] = 0.1 M at 30 °C are shown in Figs. 2 and 3. The detailed results are tabulated in Supporting information. DTAB form oblate spheroidal micelles with half axes a = 14.3 Å and b = 24.1 Å in [NaBr] = 0.1 M at 30 °C. The micelles are slightly larger as compared to what has previously been found at 40 °C and identical NaBr concentration (a = 14.0 Å and b = 23.7 Å) [7]. The data for samples with moderate fractions of DDAB were best fitted with a model for triaxial general ellipsoids (tablet-shaped micelles) with half axes $a < b < c$. In Fig. 4 we have plotted the three half axes of the general micelles against the mole fraction of DDAB in solution, $y \equiv$ [DDAB]/([DDAB] + [DTAB]), for samples with given total surfactant concentration $c_t \equiv$ [DDAB] + [DTAB]. It is seen that the micelles grow substantially in the length direction, whereas the width and thickness are rather constant with respect to surfactant mole fraction. The micelles grow in a similar manner as a sample with given overall surfactant composition (y) is diluted. The micelle growth upon dilution is due to the difference in free surfactant concentration between DDAB and DTAB, which causes a change in aggregate composition [see further below] [18].

As the micelles grow beyond about c = 100 Å, they appear to become rather polydisperse. As a result, the model fit for samples

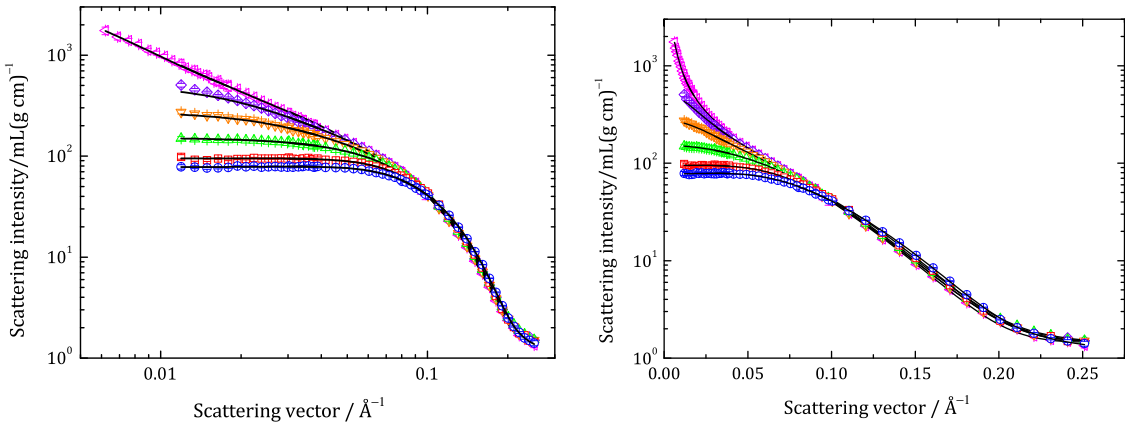

Fig. 2. Normalised scattering cross section $(d\sigma/d\Omega)/c_t$ as a function of the scattering vector q for mixtures of DDAB and DTAB in [NaBr] = 0.1 M in D_2O for a given total surfactant concentration c_t = [DDAB] + [DTAB] = 30 mM. The composition of the samples are y = [DDAB]/([DDAB] + [DTAB]) = 0 (pure DTAB, circles), y = 0.05 (squares), y = 0.10 (up triangles), y = 0.15 (down triangles), y = 0.20 (diamonds) and y = 0.25 (left triangles). Individual symbols represent SANS data obtained for different sample-detector distances. The solid lines represent the best available fit with a model for oblate spheroids (squares), general ellipsoids (circles, up and down triangles), long wormlike micelles (diamonds and left triangles). The results of the fits are given in Fig. 4 and in Supporting information. The quality of the fits as measured by χ^2 are 1.6 (squares), 2.0 (circles), 1.8 (up triangles), 3.8 (down triangles), 7.7 (diamonds) and 8.1 (left triangles). The model fit of the sample y = 0.25 (left triangles) also includes SLS data not shown in the figure [*cf.* Fig. 5]. The scattering behaviour at high q-values is emphasised by the graphs on a semi-logarithmic scale shown to the right.

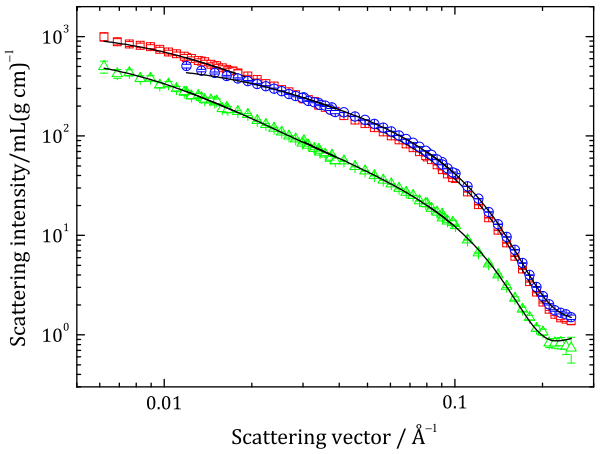

Fig. 3. Normalised scattering cross section $(d\sigma/d\Omega)/c_t$ as a function of the scattering vector q for mixtures of DDAB and DTAB in [NaBr] = 0.1 M in D_2O for a given composition y = [DDAB]/([DDAB] + [DTAB]) = 0.20. The total surfactant concentration of the samples are c_t = [DDAB] + [DTAB] = 30 mM (circles), c_t = 15 mM (squares) and c_t = 7.5 mM (up triangles). Individual symbols represent SANS data obtained for different sample-detector distances. The solid lines represent the best available fits with a model for polydisperse wormlike micelles with an elliptical cross-section. The spatial dimensions obtained from the model fits are $\langle L\rangle$ = 200 ± 10 Å, a = 13.7 ± 0.2 Å, b = 22.4 ± 0.3 Å (squares), $\langle L\rangle$ = 510 ± 40 Å, a = 14.5 ± 0.4 Å, b = 21.1 ± 0.6 Å (circles) and $\langle L\rangle$ = 1090 ± 140 Å, $a = 16.4^{+1.1}_{-2.3}$ Å, $b = 18.5^{+2.9}_{-1.0}$ Å (triangles). The quality of the fits as measured by χ^2 are 7.7 (squares), 8.1 (circles) and 1.8 (triangles).

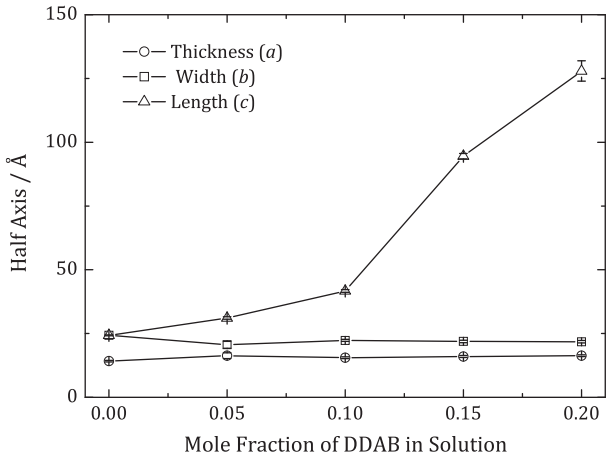

Fig. 4. Half axes related to the thickness a (circles), width b (squares) and length c (triangles), as obtained from the least square fitting analysis of SANS data for samples with mixed DDAB/DTAB micelles in [NaBr] = 0.1 M at 30 °C, plotted against the mole fraction of DDAB in solution (y) for a given total surfactant concentration c_t = [DDAB] + [DTAB] = 30 mM.

with the longest micelles could be improved using a model for long polydisperse rigid rods or flexible worms with an elliptical cross-section. The relative standard deviation $\sigma_L/\langle L\rangle$ was found to be close to unity. Comparing the fitting results (excluding structure factor effects) for the two models monodisperse ellipsoids (χ^2 = 11.9) and polydisperse rods (χ^2 = 7.7), respectively, for the sample [y = 0.20, c_t = 30 mM] shows that a half axis related to length $c \approx 130$ Å corresponds to a weight-average length of the rods $\langle L\rangle \approx 200$ Å. Notably, the DDAB/DTAB mixed micelles in [NaBr] = 0.1 M are found to be conspicuously larger as compared to what we recently found for the corresponding micelles in the absence of added salt [18]. In accordance, we observe wormlike micelles longer than 2000 Å in the presence of [NaBr] = 0.1 M (see further below), whereas tablet-shaped micelles in the absence of added salt never grow longer than about 150 Å.

The errors of the spatial dimensions as obtained from the model fitting analysis are for most cases very small. For samples with [DTAB] + [DDAB] = 30 mM, they fall in the range Δa = ±0.2–1.1 Å, Δb = ±0.3–1.4 Å and Δc = ±0.5–4 Å. The largest relative errors refer to the sample at y = 0.05, in which rather small ellipsoidal micelles are found [*cf.* Fig. 4]. The rather small errors demonstrate that the agreement between data and model become significantly improved using models for tablet-shaped or long rodlike or wormlike micelles with an elliptical cross-section. The only exception is the sample [y = 0.20, c_t = 7.5 mM], for which we are not able to conclude the presence of a noncircular cross-section, since the statistical errors of the data points are comparatively large for this rather dilute sample [see further below].

When the fraction of DDAB is increased beyond a certain value the samples become turbid and birefringent. Since an abrupt transition from micelles to large bilayer discs and vesicles was seen for the same surfactant mixture in absence of added salt [18], we

believe that the turbid phase consists of macroscopically large planar bilayers. For the three samples [$y = 0.20$, $c_t = 7.5$ mM], [$y = 0.25$, $c_t = 15$ mM] and [$y = 0.25$, $c_t = 7.5$ mM] at room temperature (23 °C), we observe a segregation or phase separation in the samples in the way that a turbid phase is gathered on top of the sample whereas the bottom part is clear. Notably, in the absence of added salt bilayer discs were frequently seen to coexist with vesicles in samples containing various bilayer structures [18]. However, in the presence of 0.1 M NaBr the bilayers most probably consist of large lamellar sheets causing the samples to appear turbid and birefringent. The sample [$y = 0.25$, $c_t = 30$ mM] becomes completely isotropic and transparent when heated to 30 °C.

In our experimental set up the neutron beam enters the bottom clear phase and the corresponding SANS data are consistent with wormlike micelles without any presence of bilayer aggregates. Combining SANS data with static light scattering (SLS) reveals that wormlike micelles larger than $\langle L \rangle \approx 2000$ Å is present in [$y = 0.25$, $c_t = 30$ mM] at 30 °C [*cf.* Fig. 5]. The intensity of the normalised scattering data is found to be somewhat lower for samples with phase separation [*cf.* Fig. 3] indicating that some of the material, i.e. the bilayer phase, does not contribute to the scattering. This means that the amount of surfactant in the measured phase must be lower than the total amount of surfactant, which explains the less good statistics of the SANS data points for the most diluted sample shown in Fig. 3.

The concentration of free DTAB coexisting with surfactant aggregates is always much larger than the concentration of free DDAB as a result of the difference in *cmc* between the two surfactants and, as a consequence, the mole fraction of DDAB in the aggregates (x) is usually different than the overall surfactant mole fraction in solution (y) [19]. We have measured *cmc* with light scattering for DTAB in H_2O and [NaBr] = 0.1 M and it is found to equal $cmc_2 = 4.3$ mM. This value is close to what has previously been reported for the same system [51]. The *cmc* for DDAB equals $cmc_1 = 0.085$ mM in absence of added salt [31] and is expected to be even lower as an additional electrolyte is added. It has recently been demonstrated that the aggregate surfactant mole fraction x may be accurately calculated from simple thermodynamic considerations [19]. The procedure of calculating x is described in Supporting information where the resulting values are tabulated.

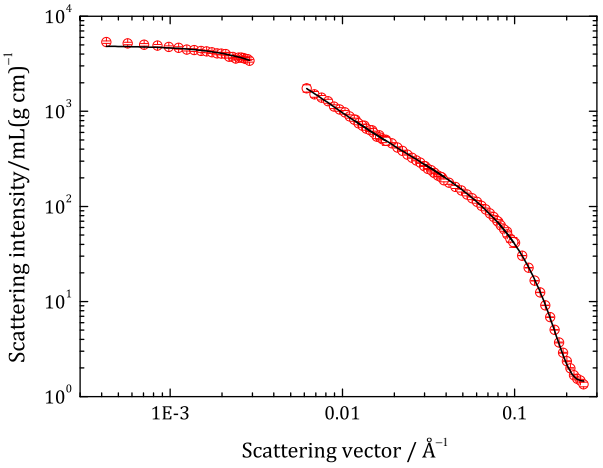

Fig. 5. Normalised scattering cross section $(d\sigma/d\Omega)/c_t$ as a function of the scattering vector q for mixtures of DTAB and DDAB in [NaBr] = 0.1 M in D_2O at 30 °C for an overall mole fraction of DDAB equal to $y = 0.25$ and given total surfactant concentration $c_t = 30$ mM. Individual symbols represent SANS data obtained for different sample-detector distances and SLS data (low-q values). The solid lines represent the best available fit with a model for wormlike micelles with an elliptical cross-section. The spatial dimensions obtained from the model fitting are $\langle L \rangle = 2290 \pm 80$ Å, $a = 14.2 \pm 0.3$ Å, $b = 21.1 \pm 0.5$ Å. The quality of the fit is $\chi^2 = 8.1$.

It is clearly seen that the growth of micelles upon decreasing the overall surfactant concentration c_t at a given overall mole fraction y is correlated to changes in x. Bilayer aggregates are present in the sample [$y = 0.25$, $c_t = 30$ mM], which become turbid at room temperature, corresponding to an aggregate mole fraction equal to $x = 0.28$. This value is substantially lower than the point of transition from micelles to bilayers, occurring at $x = 0.48$ in D_2O, that we recently found for the same surfactant mixture in absence of added salt [18]. We have also investigated the micelle-to-bilayer transition for the same mixtures in 0.1 M NaBr in the solvent H_2O. By means of simply diluting stock solutions with [DTAB] + [DDAB] = 60 mM, we may directly observe the formation of bilayers (lamellar phase) as a result of the samples instantly turning turbid and birefringent. We observe an obvious difference between mixtures in H_2O and D_2O in [NaBr] = 0.1 M. For instance, the sample [$y = 0.25$, $c_t = 30$ mM] in D_2O is turbid at 23 °C, whereas micelles are still present (clear sample) at [$y = 0.25$, $c_t = 15$ mM] in H_2O. In accordance, bilayers are observed to begin to form at a surfactant composition in the aggregates $x = 0.33$ in H_2O as compared to $x = 0.28$ in D_2O. Our results as to the micelle-to-bilayer transition for mixtures of DTAB and DDAB at some different environmental conditions, obtained in the present as well as previous works [18,19], are summarised in Table 1.

An abrupt transition from micelles to bilayers have been predicted to occur as $\xi H_0 = 1/4$, where H_0 is the spontaneous curvature and ξ is the thickness of the self-assembled interfacial aggregates [18,32]. In accordance, we may draw the following conclusions as to differences in spontaneous curvature H_0 for DDAB/DTAB mixtures at different environmental conditions: H_0 (D_2O) > H_0 (H_2O) in absence of added salt, H_0 (D_2O) < H_0 (H_2O) in 0.1 M NaBr, H_0 (absence of added salt) > H_0 (0.1 M NaBr) and H_0 (30 °C) > H_0 (23 °C) in 0.1 M NaBr. The trends with respect to electrolyte concentration and temperature are expected in accordance with the Poisson–Boltzmann theory [23,52]. The different trends for the spontaneous curvature in H_2O and D_2O, respectively, as a large amount of electrolyte is added needs to be further investigated to be fully understood. It is, however, well-known that ionic species may interact differently with solvent molecules as a result of different hydrogen bonding properties of H_2O and D_2O, respectively [53].

4.2. Mixtures of CTAB and DTAB in [NaBr] = 0.1 M

SANS data for mixtures of CTAB and DTAB in [NaBr] = 0.1 M at 30 °C for different overall mole fractions $y \equiv$ [CTAB]/([CTAB] + [DTAB]) and given total surfactant concentration $c_t \equiv$ [CTAB] + [DTAB] are shown in Fig. 6. The results from the least square model fitting data analysis are shown in Fig. 7 and tabulated in Supporting information. Most interestingly and unexpectedly, the growth behaviour with respect to surfactant composition of micelles formed by two cationic single-chain surfactants with different chain lengths appears to be completely different as compared to mixtures of a single-chain and a double-chain surfactant [*cf.* Fig. 7]. It turns out that the oblate spheroidal DTAB micelles transform into prolate spheroidal micelles as CTAB is added so as to give

Table 1
The mole fraction of DDAB in self-assembled interfacial aggregates (x) where a transition from micelles to bilayers is observed in DDAB/DTAB mixtures at some different environmental conditions.

Solvent	Temperature (°C)	Point of transition
H_2O	23	$x = 0.41$
D_2O	23	$x = 0.48$
[NaBr] = 0.1 M in H_2O	23	$x = 0.33$
[NaBr] = 0.1 M in D_2O	23	$x = 0.28$
[NaBr] = 0.1 M in D_2O	30	$x = 0.31$

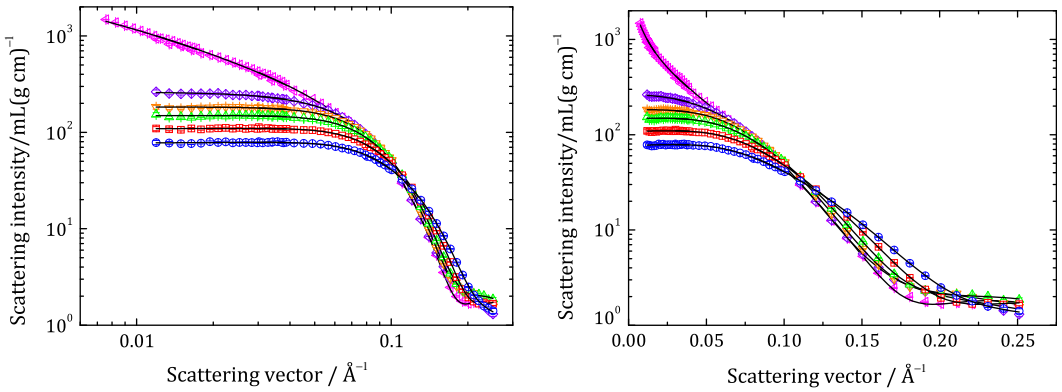

Fig. 6. Normalised scattering cross section $(d\sigma/d\Omega)/c_t$ as a function of the scattering vector q for mixtures of DTAB and CTAB in [NaBr] = 0.1 M in D_2O for a given total surfactant concentration c_t = [CTAB] + [DTAB] = 30 mM. The composition of the samples are y = [CTAB]/([CTAB] + [DTAB]) = 0 (pure DTAB, circles), y = 0.20 (squares), y = 0.40 (up triangles), y = 0.60 (down triangles), y = 0.80 (diamonds) and y = 1.0 (pure CTAB, left triangles). Individual symbols represent SANS data obtained for different sample-detector distances. The solid lines represent the best available fit with a model for oblate spheroids (squares), general ellipsoids (circles, up and down triangles and diamonds) and long polydisperse rodlike micelles (left triangles). The results of the fits are given in Fig. 7 and in Supporting information. The quality of the fits as measured by χ^2 are 1.6 (squares), 2.2 (circles), 3.7 (up triangles), 3.8 (down triangles), 4.4 (diamonds) and 23.2 (left triangles). The scattering behaviour at high q-values is emphasised by the graphs on a semi-logarithmic scale shown to the right.

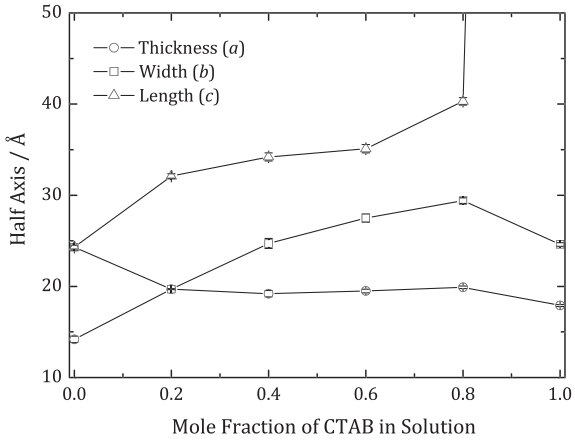

Fig. 7. Half axes related to the thickness a (circles), width b (squares) and length c (triangles), as obtained from the least square fitting analysis of SANS data of samples with mixed CTAB/DTAB micelles in [NaBr] = 0.1 M at 30 °C, plotted against the mole fraction of CTAB in solution (y) for a given total surfactant concentration c_t = [CTAB] + [DTAB] = 30 mM.

an overall solution mole fraction y = 0.20. As the fraction of CTAB is further increased the micelles grow with an approximately equal rate in both width and length directions, in sharp contrast to the growth behaviour of DDAB/DTAB mixed micelles. Notably, the thickness of the mixed micelles (half axis a) is rather constant in the interval y = 0.20–0.80 and seems to be largely determined by the longer surfactant. Because of the moderate growth in length, the mixed CTAB/DTAB micelles are rather small and compact, even at y = 0.80. However, pure CTAB micelles in [NaBr] = 0.1 M at 30 °C are found to be shaped as flexible rods or worms that are too long for their size to be determined with SANS. The considerable change in width-to-thickness ratio of CTAB/DTAB micelles is indicated in the SANS data shown in Fig. 6 by the different scattering behaviours in the range 0.1 Å^{-1} < q < 0.2 Å^{-1}.

Our results suggest that the large differences in growth rates between mixed DDAB/DTAB and CTAB/DTAB micelles are related to curvature effects. The local curvature is not changed as rodlike DDAB/DTAB micelles increases in length but not in width, allowing for a considerable growth rate of the micelles. Mixed CTAB/DTAB micelles, on the other hand, are found to increase considerably in width with surfactant composition. A change in width means that the curvature of the micelles must change during the growth process. This change in curvature implies an energetic penalty that needs to become overcome in the growth process, which explains the considerably lower growth rate observed for CTAB/DTAB micelles.

The mixed micelles are found to grow slightly upon diluting the samples as a result of the increasing fraction of aggregated CTAB. The calculated mole fraction of aggregated CTAB (x) is tabulated for the different samples in Supporting information. The difference in *cmc*s between CTAB and DTAB in [NaBr] = 0.1 M is moderate, i.e. cmc_1 = 0.55 mM (CTAB) [27] and cmc_2 = 4.3 mM (DTAB). As a result, x is less influenced by changes in total surfactant concentration in comparison with the case of DDAB/DTAB surfactant mixtures.

The errors of the geometrical dimensions for CTAB/DTAB micelles are always found to be small in magnitude. For samples with [CTAB] + [DTAB] = 30 mM, they are in the range Δa = ±0.1–0.4 Å, Δb = ±0.3–0.6 Å and Δc = ±0.3–0.5 Å [*cf.* Fig. 7].

5. Rationalising the growth of tablet-shaped micelles in terms of bending elasticity

We have recently demonstrated that the growth behaviour of triaxial general (tablet-shaped) micelles may be rationalised in terms of three bending elasticity constants as defined from the so called Helfrich-expression [54]. In accordance, the free energy of a self-assembled interfacial aggregate with interfacial area A and interfacial tension γ_0 may be calculated as

$$E = \gamma_0 A + 2k_c \int (H - H_0)^2 dA + \bar{k}_c \int K dA \qquad (2)$$

where H and K are the mean and Gaussians curvatures, respectively. The general micelle model relates the width (b) and length (c) of tablet-shaped micelles with the three bending elasticity constants bending rigidity (k_c), spontaneous curvature (H_0) and saddle splay constant ($\bar{k}_c$), respectively [32]. However, in order to determine all three bending elasticity constants uniquely from our experimental data, an additional quantity to a and b is needed. Therefore, we have chosen to fix the parameter $\beta \equiv \pi k_c(1 - 4\xi H_0)/kT + 2\pi\lambda$ to zero, which is reasonable for a given surfactant concentration [18]. $\lambda \equiv \xi^2 \gamma_p / kT$ is the reduced and γ_p the real planar interfacial tension of a self-assembled interfacial aggregate with thickness ξ. It was demonstrated that the magnitude of β influence the absolute values of $k_c H_0$, k_c and $\bar{k}_c$, but not the trends and how they are influenced by

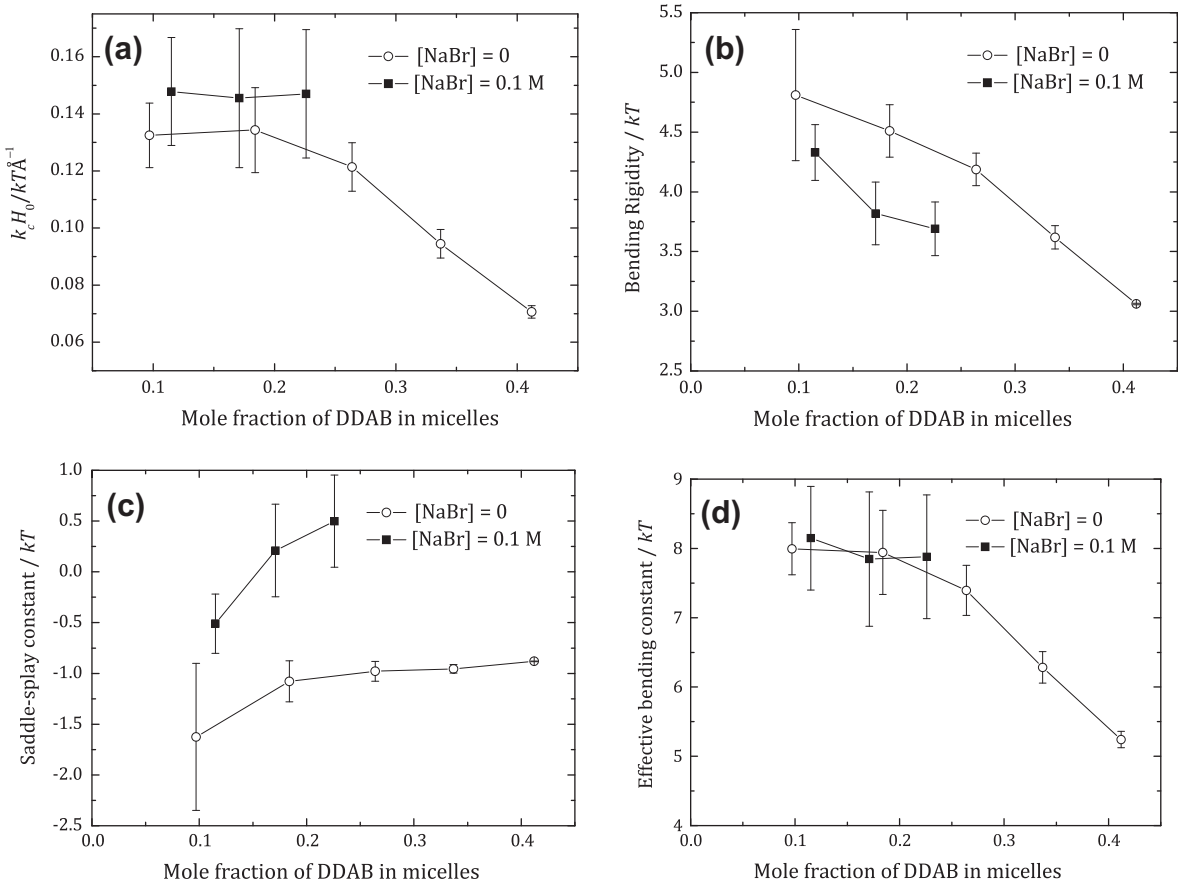

Fig. 8. Bending elasticity constants, as obtained from the fitting parameters b and c plotted against the mole fraction of aggregated DDAB (x) for a given value of the thermodynamic parameter $\beta = 0$. Open symbols refer to DDAB/DTAB mixtures in absence of added salt at 23 °C and taken from Ref. [18]. Solid symbols refer to DDAB/DTAB mixtures in [NaBr] = 0.1 M at 30 °C. (a) Bending rigidity (k_c) times the spontaneous curvature (H_0), (b) bending rigidity (k_c), (c) saddle-splay constant ($\bar{k}_c$), (d) effective bending constant ($k_{eff} \equiv 2k_c + \bar{k}_c$). Open symbols correspond to samples with $y = 0.05$, 0.10, 0.15, 0.20 and 0.20 at $c_t = 30$ mM. Solid symbols correspond to samples with $y = 0.10$, 0.15 and 0.20 at $c_t = 30$ mM. The statistical errors were evaluated from the errors in spatial dimensions as obtained from SANS data analysis.

the addition of inert salt as well as type of surfactant mixture [18]. We may note that it is, from a molecular point of view, easier to interpret k_cH_0 than H_0 since k_cH_0 is directly related to the first moment in curvature, whereas $H_0 \equiv k_cH_0/k_c$ is the ratio between the first and second moments with respect to H [23,55,56]. Unlike the critical packing parameter, the bending elasticity approach explicitly takes into account that chemical structure of surfactant molecules, surfactant composition, electrolyte concentration, etc. influences the curvature (equivalent to aggregate size and shape) of the self-assembled interfacial aggregates.

The procedure to deduce k_cH_0, k_c and $\bar{k}_c$ from experimentally obtained half-axes of ellipsoidal micelles has been described in detail in a recent paper by ours [18], in which the growth behaviour with respect to surfactant composition of micelles formed in mixtures of DDAB and DTAB in the absence of added salt were analysed. We were able to conclude that tablet-shaped micelles grow in the length direction mainly as a result of the reduction of the bending rigidity k_c, whereas they grow in width mainly as a result of decreasing k_cH_0. The bending rigidity was found to mainly determine the shape of micelles in so far low k_c-values favour geometrically heterogeneous elongated micelles, whereas high values of k_c favours less heterogeneous and more compact geometries. The saddle-splay constant $\bar{k}_c$ has an indirect influence on the size of self-assembled interfacial aggregates in so far the size of micelles is expected to increase with increasing values of $\bar{k}_c$.

In Fig. 8 we have plotted the various bending elasticity constants, as estimated from the model fitting results, for the DDAB/DTAB mixtures $y = 0.10$, 0.15 and 0.20 at a constant overall surfactant concentration $c_t = 30$ mM in [NaBr] = 0.1 M. To illustrate the effect of adding salt to the system, we have also included our previously obtained results for DDAB/DTAB in absence of added salt. In order to facilitate the comparison, we have plotted all quantities against the mole fraction of DDAB in the aggregates (x). It is seen that the errors of the different bending elasticity constants, as calculated from the errors of ellipsoid half axes obtained from our model fitting analysis, increases in magnitude as the micelles approaches spheroidal shape and, as a consequence, it is not possible to determine k_cH_0, k_c and $\bar{k}_c$ for the rather small spheroidal micelles at $y = 0$ and 0.05. The wormlike micelles at [$y = 0.25$, $c_t = 30$ mM] are too large and polydisperse to be fitted with an ellipsoidal model. For the three samples for which the bending elasticity constants were deduced ($y = 0.10$, 0.15 and 0.20), we do not observe any clear trend of k_cH_0 in the same way as we did for the case of the considerably smaller and more compact DDAB/DTAB micelles in absence of added salt [*cf.* Fig. 8a]. Notably, the errors in k_cH_0 are comparatively large in magnitude mainly as a result of the rather small axial ratios b/a for DDAB/DTAB mixed micelles in [NaBr] = 0.1 M. Nevertheless, we are able to conclude from the shift in surfactant composition in the aggregates, where a micelle-to-bilayer transition occurs [see above], that the spontaneous curvature H_0 is significantly reduced upon adding salt to the mixtures.

It is easier to evaluate the influence of electrolyte concentration on the bending rigidity k_c and the saddle-splay constant $\bar{k}_c$. It is obvious that the main effect of adding salt is a significant reduction

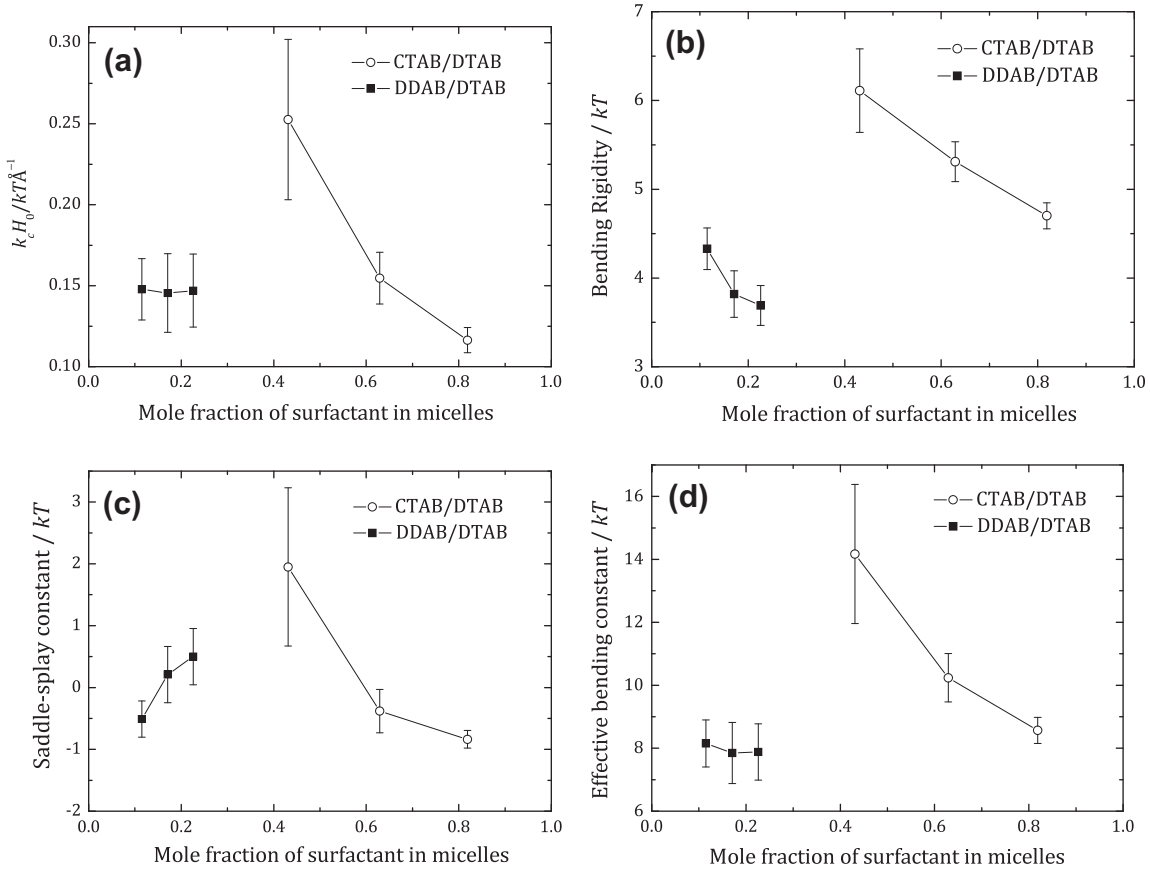

Fig. 9. Bending elasticity constants, as obtained from the fitting parameters b and c plotted against the mole fraction of aggregated CTAB (open symbols) or DDAB (solid symbols) for a given value of the thermodynamic parameter $\beta = 0$. Open symbols refer to CTAB/DTAB and solid symbols refer to DDAB/DTAB mixtures in [NaBr] = 0.1 M at 30 °C. (a) Bending rigidity (k_c) times the spontaneous curvature (H_0), (b) bending rigidity (k_c), (c) saddle-splay constant ($\bar{k}_c$), (d) effective bending constant ($k_{eff} \equiv 2k_c + \bar{k}_c$). Open symbols correspond to the samples $y = 0.40$, 0.60 and 0.80 at $c_t = 30$ mM. Solid symbols correspond to the samples $y = 0.10$, 0.15 and 0.20 at $c_t = 30$ mM. The statistical errors were evaluated from the errors in spatial dimensions as obtained from SANS data analysis.

of k_c together with an increase of $\bar{k}_c$ [*cf.* Fig. 8b and c]. The reduction of the bending rigidity favours considerably elongated micelles and promotes the growth in length direction. The saddle-splay constant primarily influences the size of the micelles, but not the shape, as a result of the Gauss–Bonnet theorem [32]. As a consequence, an increase of electrolyte concentration promote the growth of micelles, which are found to be considerably larger in [NaBr] = 0.1 M as compared to the case of absence of added salt. Hence, the different values for k_c and $\bar{k}_c$ in absence and presence of added salt, respectively, explains the completely different sizes observed for micelles at the micelle-to-bilayer transition, where $H_0 = 1/4\xi$ is expected to be equal in magnitude, for the two cases. This observation cannot be rationalised by means of using, for instance, a single *cpp* parameter. It has been demonstrated that a decrease of k_c, as well as an increase in $\bar{k}_c$, with increasing electrolyte concentration follows from the Poisson–Boltzmann mean field theory [52,57]. More recently, it was shown that those trends are enhanced if effects due to the self-assembled interface having a finite thickness are taken into account [23].

In Fig. 9 we compare the trends of the different bending elasticity constants, as functions of aggregated surfactant mole fractions, between mixtures of CTAB/DTAB and DDAB/DTAB dissolved in [NaBr] = 0.1 M at 30 °C and a given total surfactant concentration equal to 30 mM. The three samples for CTAB/DTAB mixtures correspond to overall mole fractions of CTAB equal to $y = 0.40$, 0.60 and 0.80, i.e. samples the data of which were best fitted with a model for triaxial general ellipsoids. At $y = 0.20$, the micelles are rather small and strictly prolate and it is not possible to determine the bending elasticity constants from the general micelle model. Long wormlike micelles, too large for their size to be determined from our SANS data, are formed in samples with pure CTAB in [NaBr] = 0.1 M, and the corresponding data could not be fitted with the general ellipsoidal model.

As a result of the significant growth in width of the micelles, the spontaneous curvature (or rather $k_c H_0$) is seen to decrease with an increasing fraction of CTAB in mixed CTAB/DTAB micelles [*cf.* Fig. 9a]. Likewise, the growth in length direction of the micelles is mainly the result of a decreasing bending rigidity with an increasing fraction of aggregated CTAB [*cf.* Fig. 9b]. It may be noted that the fact that DTAB form small oblate micelles, whereas CTAB form long wormlike micelles in [NaBr] = 0.1 M, implies that CTAB must have a substantially lower k_c value than DTAB. This difference is also manifested by the completely different growth rates of DTAB and CTAB with respect to surfactant concentration in presence of [NaBr] = 0.1 M [7,27]. As a matter of fact, recent model calculations have demonstrated that k_c is expected to have a distinct maximum value as a function of the hydrophilic–lipophilic balance (HLB) of a surfactant molecule [56]. The transformation from oblate spheroidal DTAB micelles to prolate spheroidal mixed CTAB/DTAB micelles at $y = 0.20$ is intriguing. Unfortunately, the micelles in this regime are too small in order to deduce the various bending elasticity constants from the general micelle model. Nevertheless, it is suggested by our arguments that the oblate-to-prolate transformation is mainly a result of a reduction of the bending rigidity following from the fact that CTAB has a significantly lower k_c than DTAB.

The saddle-splay constant shows completely different trends as either a double-chain surfactant (DDAB) or a surfactant with longer tail (CTAB) is added to DTAB solutions in [NaBr] = 0.1 M [*cf.* Fig. 9c]. In the latter case, $\bar{k}_c$ is found to increase with increasing fraction of aggregated CTAB, and the growth of mixed CTAB/DTAB micelles is demoted. As a result, mixed CTAB/DTAB micelles are found to be small and compact as compared to large wormlike mixed DDAB/DTAB micelles present in [NaBr] = 0.1 M.

In addition, we have plotted the effective bending constant $k_{eff} \equiv 2k_c + \bar{k}_c$ for the surfactant mixtures in Figs. 8d and 9d. The size of self-assembled interfacial aggregates is expected to increase with increasing values of k_{eff}, which must be a positive quantity for aggregates to form at all [58]. Although k_c and $\bar{k}_c$ for DTAB/DDAB mixtures are completely different in the absence of added salt and in [NaBr] = 0.1 M, respectively, $k_{eff} \equiv 2k_c + \bar{k}_c$ is found to be rather unaffected by electrolyte concentration. The behaviour of k_{eff} as a function of x shown in Figs. 8d and 9d is very similar to the corresponding behaviours of $k_c H_0$ in Figs. 8a and 9a, respectively.

6. Conclusions

Surfactant micelles have conventionally been considered to grow only in one direction, in a "ladder model", from small spherical to larger spherocylindrical micelles [22,59,60]. In contrast to this behaviour, however, recent small-angle neutron scattering (SANS) measurements have indicated that ordinary surfactant micelles may be shaped as triaxial general tablets with distinct thickness, width and length, respectively [7,13,18]. In the present paper, we have followed up our earlier discoveries and focused on the growth behaviours of mixed micelles with respect to surfactant composition. We have chosen to study two surfactant mixtures that display completely different growth rates in [NaBr] = 0.1 M, with the specific aim to correlate the corresponding growth behaviours with the geometrical structure of the micelles. In accordance, mixed CTAB/DTAB micelles are found to grow slightly, and with an approximately equal rate, in length and width directions, from biaxial prolate spheroidal micelles to, still comparatively small and compact, triaxial general ellipsoids. Mixed DDAB/DTAB micelles, on the other hand, grow significantly in length, but not at all in width, to elongated rodlike and giant wormlike micelles. Likewise, the size of DDAB/DTAB micelles in presence of [NaBr] = 0.1 M is found to be more than fifteen times larger than in absence of added salt.

The structural behaviours of the mixed micelles indicate that curvature effects are of crucial importance for the different growth rates. The local curvature in mixed DDAB/DTAB micelles, in presence of brine, does not need to change during the growth process as the micelles grow exclusively in the length direction and, as a consequence, the micelles may grow with a large rate into giant wormlike micelles. Mixed CTAB/DTAB micelles, on the other hand, grow with respect to both width and length, which means that the local curvature in the end caps changes considerably during the growth process. As a consequence, the growth rate is low and mixed CTAB/DTAB micelles are found to be consistently rather small and compact. Hence, we are able to conclude that the different growth behaviours with respect to width and length, respectively, may explain the significantly different growth rates in size displayed by the two investigated surfactant mixtures. Moreover, our analyses of the experimental results in terms of bending elasticity properties demonstrate that the main effect of adding an inert salt to a surfactant mixture is to reduce spontaneous curvature and bending rigidity, whereas the saddle-splay constant is increased. Likewise, differences in growth behaviours between CTAB/DTAB and DDAB/DTAB mixed micelles, respectively, are found to mainly depend on different trends with respect to bending rigidity and saddle-splay constant.

Acknowledgments

This work was supported by the Swedish Research Council. The SANS measurements were supported by the European Commission (Grant Agreement N 226507-NMI3).

Appendix A. Supplementary material

Supplementary data associated with this article can be found, in the online version, at http://dx.doi.org/10.1016/j.jcis.2012.05.015.

References

[1] C. Tanford, The Hydrophobic Effect, Wiley, New York, 1980.
[2] D.W.R. Gruen, Prog. Colloid Polym. Sci. 70 (1985) 6.
[3] H.V. Tartar, J. Phys. Chem. 59 (1955) 1195.
[4] C. Tanford, J. Phys. Chem. 76 (1972) 3020.
[5] S.S. Berr, J. Phys. Chem. 91 (1987) 4760.
[6] S.S. Berr, R.R.M. Jones, Langmuir 4 (1988) 1247.
[7] M. Bergström, J.S. Pedersen, Phys. Chem. Chem. Phys 1 (1999) 4437.
[8] M. Bergström, U.R.M. Kjellin, P.M. Claesson, I. Grillo, J. Phys. Chem. B 108 (2004) 1874.
[9] P. Lianos, R. Zana, J. Colloid Interface Sci. 84 (1981) 100.
[10] P. Lianos, J. Lang, R. Zana, J. Colloid Interface Sci. 91 (1983) 276.
[11] M. Corti, V. Degiorgio, Chem. Phys. Lett. 53 (1978) 237.
[12] H. Pilsl, H. Hoffmann, S. Hoffmann, J. Kalus, A.W. Kencono, P. Lindner, W. Ulbricht, J. Phys. Chem. 97 (1993) 2745.
[13] M. Bergström, J.S. Pedersen, Langmuir 15 (1999) 2250.
[14] M. Bergström, J.S. Pedersen, J. Phys. Chem. B 103 (1999) 8502.
[15] M. Bergström, J.S. Pedersen, J. Phys. Chem. B 104 (2000) 4155.
[16] M. Kadi, P. Hansson, M. Almgren, M. Bergström, V.M. Garamus, Langmuir 20 (2004) 3933.
[17] K.M. Lusvardi, A.P. Full, E.W. Kaler, Langmuir 11 (1995) 487.
[18] L.M. Bergström, S. Skoglund, K. Danerlöv, V.M. Garamus, J.S. Pedersen, Soft Matter 7 (2011) 10935.
[19] L.M. Bergström, M. Aratono, Soft Matter 7 (2011) 8870.
[20] I. Grillo, J. Penfold, I. Tucker, F. Cousin, Langmuir 25 (2009) 3932.
[21] I. Grillo, J. Penfold, Langmuir 27 (2011) 7453.
[22] J.N. Israelachvili, D.J. Mitchell, B.W. Ninham, J. Chem. Soc., Faraday Trans. 2 72 (1976) 1525.
[23] L.M. Bergström, Langmuir 22 (2006) 3678.
[24] A. Malliaris, J. Lang, R. Zana, J. Chem. Soc., Faraday Trans. 1 82 (1986) 109.
[25] R. Zana, in: D.N. Rubingh, P.M. Holland (Eds.), Cationic Surfactants, Physical Chemistry, Marcel Dekker, Inc., New York and Basel, 1991, p. 41.
[26] D. Danino, Y. Talmon, R. Zana, Langmuir 11 (1995) 1448.
[27] T. Imae, R. Kamiya, S. Ikeda, J. Colloid Interface Sci. 108 (1985) 215.
[28] M.T. Yatcilla, K.L. Herrington, L.L. Brasher, E.W. Kaler, S. Chiruvolu, J.A.N. Zasadzinski, J. Phys. Chem. 100 (1996) 5874.
[29] M. Bergström, J.S. Pedersen, Langmuir 14 (1998) 3754.
[30] M. Bergström, J.S. Pedersen, P. Schurtenberger, S.U. Egelhaaf, J. Phys. Chem. B 103 (1999) 9888.
[31] M. Aratono, N. Onimaru, Y. Yoshikai, M. Shigehisa, I. Koga, K. Wongwailikhit, A. Ohta, T. Takiue, B. Lhoussaine, R. Strey, Y. Takata, M. Villeneuve, H. Matsubara, J. Phys. Chem. B 111 (2007) 107.
[32] L.M. Bergström, ChemPhysChem 8 (2007) 462.
[33] J.P. Cotton, in: P. Lindner, T. Zemb (Eds.), Neutron, X-Ray and Light Scattering: Introduction to an Investigative Tool For Colloidal and Polymeric Systems, North-Holland, Amsterdam, 1991, pp. 11–19.
[34] J.S. Pedersen, J. Phys. IV (Paris) Coll. C8 3 (1993) 491.
[35] J.S. Pedersen, D. Posselt, K. Mortensen, J. Appl. Crystallogr. 23 (1990) 321.
[36] B.R. Bevington, Data Reduction and Error Analysis for Physical Sciences, McGraw-Hill, New York, 1969.
[37] J.S. Pedersen, Adv. Colloid Interface Sci. 70 (1997) 171.
[38] J.M. Corkill, J.M. Goodman, T. Walker, Trans. Faraday Soc. 63 (1967) 768.
[39] Y. Chevalier, T. Zemb, Rep. Prog. Phys. 53 (1990) 279.
[40] B. Cabane, R. Duplessiz, T. Zemb, J. Phys. France 46 (1985) 2161.
[41] J.C. Eriksson, S. Ljunggren, U. Henriksson, J. Chem. Soc., Faraday Trans. 2 81 (1985) 833.
[42] J.B. Hayter, J. Penfold, Mol. Phys. 42 (1981) 109.
[43] J.P. Hansen, J.B. Hayter, Mol. Phys. 46 (1982) 651.
[44] M. Kotlarchyk, S.H. Chen, J. Chem. Phys. 79 (1983) 2461.
[45] J.B. Hayter, J. Penfold, Colloid Polym. Sci. 261 (1983) 1027.
[46] T. Neugebauer, Ann. Phys. Leipzig 42 (1943) 509.
[47] J.S. Pedersen, P. Schurtenberger, Macromolecules 29 (1996) 7602.
[48] L.M. Bergström, in: M. Tadashi (Ed.), Application of Thermodynamics to Biological and Material Science, InTech, Rijeka, 2011, pp. 289.
[49] J.C. Eriksson, S. Ljunggren, J. Chem. Soc., Faraday Trans. 2 81 (1985) 1209.
[50] D.W.R. Gruen, J. Phys. Chem. 89 (1985) 153.

[51] E.W. Anacker, R.M. Rush, J.S. Johnsson, J. Phys. Chem. 68 (1964) 81.
[52] J. Daicic, A. Fogden, I. Carlsson, H. Wennerstrom, B. Jonsson, Phys. Rev. E 54 (1996) 3984.
[53] Y. Marcus, Ion Properties, Marcel Dekker, New York, Basel, Hong Kong, 1997.
[54] W. Helfrich, Z. Naturforsch. C 28 (1973) 693.
[55] L.M. Bergström, Langmuir 22 (2006) 6796.
[56] L.M. Bergström, Langmuir 25 (2009) 1949.
[57] D.J. Mitchell, B.W. Ninham, Langmuir 5 (1989) 1121.
[58] L.M. Bergström, Colloids Surf., A 316 (2008) 15.
[59] P.J. Missel, N.A. Mazer, G.B. Benedek, C.Y. Young, J. Phys. Chem. 84 (1980) 1044.
[60] J.N. Israelachvili, Intermolecular and Surface Forces, third ed., Academic Press, 2011.